Chemical Science

ROYAL SOCIETY OF CHEMISTRY

EDGE ARTICLE

View Article Online
View Journal | View Issue

Check for updates

Cite this: *Chem. Sci.*, 2020, **11**, 786

All publication charges for this article have been paid for by the Royal Society of Chemistry

Atomically dispersed Fe atoms anchored on COF-derived N-doped carbon nanospheres as efficient multi-functional catalysts†

Shengjie Wei,‡[a] Yu Wang,‡[b] Wenxing Chen,[c] Zhi Li,*[a] Weng-Chon Cheong,[a] Qinghua Zhang,[d] Yue Gong,[d] Lin Gu,[d] Chen Chen,[a] Dingsheng Wang,[a] Qing Peng[a] and Yadong Li*[a]

Non-noble metal isolated single atom site (ISAS) catalysts have attracted much attention due to their low cost, ultimate atom efficiency and outstanding catalytic performance. Herein, atomically dispersed Fe atoms are prepared by a covalent organic framework (COF)-absorption–pyrolysis strategy. The obtained Fe ISASs anchored on COF-derived N-doped carbon nanospheres (Fe-ISAS/CN) served as a multi-functional catalyst in electro-catalysis and organic catalysis, exhibiting better catalytic performance than commercial Pt/C for the ORR with good stability and methanol tolerance. Besides electro-catalysis, the Fe-ISAS/CN also showed outstanding catalytic performance in organic reactions, such as the selective oxidation of ethylbenzene to acetophenone and dehydrogenation of 1,2,3,4-tetrahydroquinoline with excellent reactivity, selectivity, stability and recyclability. Co and Ni ISAS materials can also be prepared by this method, suggesting that it is a general strategy to obtain metal ISAS catalysts. This work will provide new insight into the design of COF-derived metal ISAS multi-functional catalysts for electro-catalysis and organic reactions using rationally designed synthetic routes and the optimized structure of substrates.

Received 4th October 2019
Accepted 29th November 2019

DOI: 10.1039/c9sc05005a

rsc.li/chemical-science

Open Access Article. Published on 30 November 2019. Downloaded on 8/23/2024 6:18:58 AM.
This article is licensed under a Creative Commons Attribution-NonCommercial 3.0 Unported Licence.

Introduction

Recently, metal isolated single-atom site (ISAS) catalysts as a new frontier of catalysis has attracted much interest owing to the ultimate atom utilization efficiency and outstanding catalytic performance.[1–4] In particular, non-noble metal ISASs anchored on carbon-based substrates have been extensively utilized in electro-catalysis[5,6] and organic reactions.[7–13] However, the development of multi-functional non-noble metal ISASs which can catalyze both electro-catalysis and organic reactions has rarely been reported. Therefore, it is significant and challenging to design multi-functional non-noble metal ISAS catalysts with excellent catalytic performance not only in electro-catalysis but also in organic reactions. Besides, it is meaningful to rationally design the synthetic route and optimize the structure of the supports in order to dramatically boost the catalytic performance of metal ISASs and to reduce the usage of metal elements and catalyst cost but this is a great challenge.

Nitrogen doped carbon-based (CN) nanomaterials, serving as a common and efficient support in electro-catalysis due to their outstanding conductivity, are usually utilized to prepare metal ISAS catalysts, in which nitrogen atoms serve as anchoring sites to stabilize metal atoms.[6,14] Nitrogen doped carbon can usually be obtained by pyrolyzing nitrogenous precursors, such as MOFs,[15–19] COFs,[20,21] polymers[22,23] and small organic molecules.[24,25] However, metal ISASs anchored on COF-derived CN materials have rarely been studied. COF materials have widely been applied in gas storage and separation,[26–28] energy conversion[29,30] and catalysis[31–33] since the concept of COFs was initially proposed by Yaghi's group.[34] Compared with MOFs, COF materials are metal-free after pyrolysis. Therefore, compared with metal ISASs anchored on MOF-derived N-doped carbon, it is much easier to characterize and determine the catalytic role of metal ISASs anchored on COF-derived N-doped carbon, effectively avoiding the disturbance from metal elements as impurities from supports.

Herein, we prepare atomically dispersed Fe atoms anchored on COF-derived N-doped carbon nanospheres by a COF-absorption–pyrolysis strategy. The obtained Fe-ISAS/CN

[a]*Department of Chemistry, Tsinghua University, Beijing 100084, China. E-mail: zhili@mail.tsinghua.edu.cn; ydli@mail.tsinghua.edu.cn*

[b]*Shanghai Synchrotron Radiation Facility, Shanghai Institute of Applied Physics, Chinese Academy of Sciences, Shanghai 201800, China*

[c]*Beijing Key Laboratory of Construction Tailorable Advanced Functional Materials and Green Applications, School of Materials Science and Engineering, Beijing Institute of Technology, Beijing 100081, China*

[d]*Beijing National Laboratory for Condensed Matter Physics, Institute of Physics, Chinese Academy of Sciences, Beijing 100190, China*

† Electronic supplementary information (ESI) available. See DOI: 10.1039/c9sc05005a

‡ These authors contributed equally to this work.

This journal is © The Royal Society of Chemistry 2020

Open Access Article. Published on 30 November 2019. Downloaded on 8/23/2024 6:18:58 AM.
This article is licensed under a Creative Commons Attribution-NonCommercial 3.0 Unported Licence.

exhibited better catalytic performance for the ORR in alkaline media with a half-wave potential of 0.861 V, which is 21 mV more positive than that of commercial 20 wt% Pt/C, and showed good stability and good methanol tolerance. Besides electro-catalysis, the Fe-ISAS/CN also exhibited excellent catalytic performance in catalyzing organic reactions. In the selective oxidation of ethylbenzene to acetophenone and dehydrogenation of 1,2,3,4-tetrahydroquinoline to quinoline, the Fe-ISAS/CN showed high reactivity, high selectivity and good recyclability. Although many Fe ISAS catalysts have been widely used in the ORR[5,6,22,35–37] and organic reactions,[7,8] Fe ISAS catalysts as multi-functional catalysts in both electro-catalysis and organic reactions have rarely been reported. The multi-functional Fe-ISAS/CN derived from Fe ion-doped COFs will provide new insight into the synthesis of multi-functional catalysts not only for electro-catalysis but also for organic catalysis and the usage of COFs as the precursors of supports to anchor metal ISASs. Co and Ni-ISAS/CN can also be achieved by this method, demonstrating that it is a general strategy to prepare metal ISAS catalysts.

Compared with previously reported metal ISAS catalysts anchored on CN substrates, the Fe-ISAS/CN can serve as a multi-functional catalyst not only in electro-catalysis but also in organic reactions. Therefore, it is necessary to explore the uniqueness of the synthetic method and the structure of the catalyst. For the synthesis, the "COF-absorption–pyrolysis" strategy is simple and robust. During catalysis, the sole existence of metal ISASs without metal elements as impurities from the substrate can effectively prevent the disturbance from metal elements as impurities. Besides, the morphology and size distribution of the substrate also play an important role in catalysis. The RT-COF-1 nanospheres and the corresponding N-doped carbon nanospheres have homogeneous size distribution and morphology, with good dispersivity in liquid solvents, facilitating the absorption of metal precursors during synthesis and the exposure of metal ISASs during catalysis, improving the molecular contact between the catalytically active sites and reactants and further boosting the catalytic performance of metal ISASs. Therefore, the combination of the rational "COF-absorption–pyrolysis" strategy and the homogeneous size distribution and morphology of the substrate synergistically and effectively boosts the catalytic performance of Fe-ISAS/CN not only in electro-catalysis but also in catalyzing organic reactions.

In brief, the "COF-absorption–pyrolysis" strategy utilizes the COF material as a precursor to anchor metal ISASs, which has rarely been reported, providing new insight into the rational design of metal ISASs anchored on COFs or COF-derived substrates. The absence of metal elements from COFs and COF-derived CN facilitates the characterization and investigation of the catalytic mechanism of metal ISAS active sites, effectively avoiding the disturbance from the metal elements as impurities from substrates. Compared with other Fe-based ISAS catalysts, which can only catalyze electro-catalysis or organic reactions, the Fe-ISAS/CN in our work can serve as a multi-functional catalyst not only in electro-catalysis but also in organic reactions, providing new insight into the design of multi-functional catalysts for electro-catalysis and organic reactions using rationally designed synthetic routes and the optimized structure of the substrates.

Results and discussion

The synthesis procedure is illustrated in Fig. 1a. Firstly, RT-COF-1 was obtained by a simple and robust method at room temperature in several minutes. 1,3,5-tris(4-aminophenyl) benzene and 1,3,5-benzenetricarboxaldehyde serving as monomers were polymerized in an acidic medium. Then, metal ions were incorporated into RT-COF-1 by coordination between metal ions and nitrogen atoms in RT-COF-1. After pyrolysis under an inert atmosphere, metal ISASs were stably anchored on COF-derived N-doped carbon nanospheres. The N-doped carbon nanospheres maintained the original morphology and size distribution of RT-COF-1 after pyrolysis. As shown in Fig. 1b–d and Fig. S1–S3,† no metal nanoparticles were found in the HAADF-STEM images after pyrolysis. The corresponding energy dispersive X-ray spectroscopy elemental maps showed that C, N and metal (Fe, Co and Ni) elements were distributed

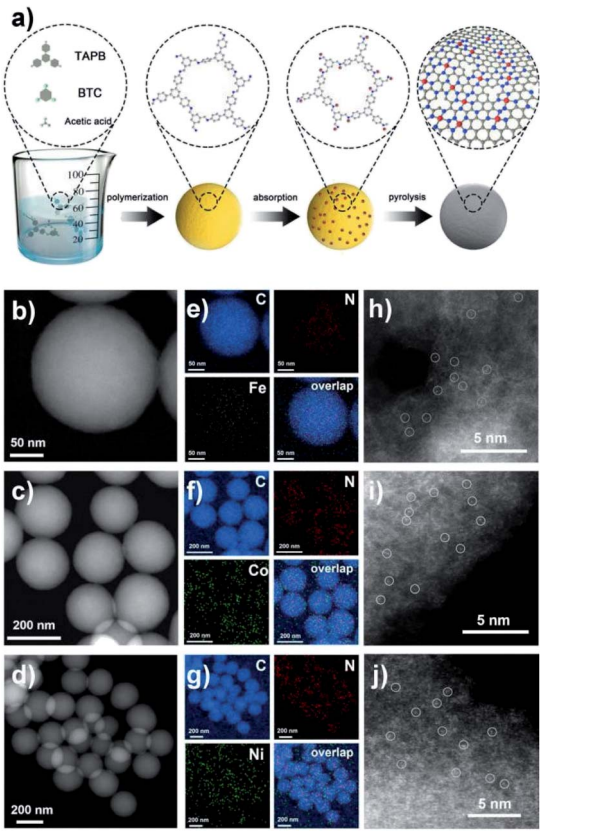

Fig. 1 (a) Schematic illustration of the synthetic process of metal ISASs anchored on COF-derived N-doped carbon nanospheres. (b)–(d) HAADF-STEM images of Fe-ISAS/CN, Co-ISAS/CN and Ni-ISAS/CN, respectively. (e)–(g) Corresponding energy dispersive X-ray spectroscopy elemental mapping results of Fe-ISAS/CN, Co-ISAS/CN and Ni-ISAS/CN, respectively. (h)–(j) AC-STEM images of Fe-ISAS/CN, Co-ISAS/CN and Ni-ISAS/CN, respectively; metal ISASs are highlighted with white circles for better observation.

Open Access Article. Published on 30 November 2019. Downloaded on 8/23/2024 6:18:58 AM.
This article is licensed under a Creative Commons Attribution-NonCommercial 3.0 Unported Licence.

homogeneously on the substrate (Fig. 1e–g). Inductively coupled plasma optical emission spectrometry (ICP-OES) measurement also demonstrated the existence of metal elements (Table S1†). The X-ray diffraction (XRD) patterns of Fe, Co and Ni-ISAS/CN only had two broad peaks around 25° and 44°, which were attributed to the characteristic carbon (002) and (100)/(101) diffractions (Fig. S4–S6†). Fe, Co and Ni ISASs were directly observed by aberration-corrected scanning transmission electron microscopy (AC-STEM) measurement as shown in Fig. 1h–j and Fig. S7–S9,† respectively. The metal ISASs, which were labelled using white circles, were atomically dispersed on the CN substrate.

To gain a better understanding of the structure of Fe-ISAS/CN at the atomic level, X-ray absorption near-edge structure (XANES) and extended X-ray absorption fine structure (EXAFS) were performed. The position of the near-edge absorption energy of Fe-ISAS/CN was located between those of Fe foil and α-Fe_2O_3, indicating that the Fe element of Fe-ISAS/CN carried a partial positive charge (Fig. 2a). The curves in *R* space of Fourier transform EXAFS (FT-EXAFS) spectra are exhibited in Fig. 2b. Compared with those for Fe foil and α-Fe_2O_3, there was only one dominant peak around 1.5 Å, which was assigned to the Fe–N/C bond, indicating the atomic dispersion of the Fe element. By contrast, there was a prominent peak located at 2.3 Å in the curve of Fe foil, which was attributed to the Fe–Fe bond. The two dominant peaks around 1.5 Å and 3.0 Å in the curve of α-Fe_2O_3 were attributed to the Fe–O bond and Fe–Fe bond, respectively. We performed quantitative EXAFS fitting to determine the coordination number of Fe-ISAS/CN. Based on the fitting results in *R* space and *k* space (Fig. 2c and d, Table S2†), the coordination number of Fe-ISAS/CN was 4.1. Therefore, the atomic dispersion of Fe-ISAS/CN was well-confirmed by combining the analysis of AC-STEM observation and EXAFS measurement. The XANES and EXAFS measurement results of Co-ISAS/CN and Ni-ISAS/CN are exhibited in Fig. S10 and S11,† respectively.

We investigated the ORR activity of Fe-ISAS/CN by using a three-electrode system in an O_2-saturated 0.1 M KOH solution. The Fe-ISAS/CN exhibited better ORR catalytic performance with a more positive half-wave potential ($E_{1/2}$ = 0.861 V) and higher kinetic current density at 0.85 V (J_k = 5.47 mA cm^{-2}), compared with commercial 20 wt% Pt/C ($E_{1/2}$ = 0.840 V, J_k = 4.53 mA cm^{-2}) (Fig. 3a and b). The comparison of ORR catalytic performance between Fe-ISAS/CN and other reported Fe-based electrocatalysts is listed in Table S3.† By contrast, the N-doped carbon nanospheres (CNs) after pyrolysis of pure RT-COF-1 without Fe loading exhibited a very poor ORR activity with an $E_{1/2}$ of 0.633 V, proving that the active sites of the ORR were Fe species rather than the CN substrate. When we increased the Fe loading supported on RT-COF-1, appreciable amounts of Fe nanoparticles supported on CN (Fe/CN) were formed after pyrolysis, which was confirmed by HAADF-STEM observation (Fig. S12†). The ORR performance of Fe/CN showed an obvious decay with an $E_{1/2}$ of 0.812 V, 49 mV negative than that of Fe-ISAS/CN, demonstrating the superior catalytic performance of Fe-ISAS/CN compared to Fe/CN in the ORR. The linear sweep voltammetry (LSV) measurement at different rotating rates demonstrated that the Fe-ISAS/CN underwent a four-electron ORR pathway (Fig. 3c) and the H_2O_2 yield of Fe-ISAS/CN was investigated by using a rotating ring disk electrode (Fig. S13†). As shown in Fig. 3d, the Fe-ISAS/CN had a Tafel slope of 78 mV dec^{-1} similar to that of commercial 20 wt% Pt/C (79 mV dec^{-1}). To evaluate the stability of the catalysts, the Fe-ISAS/CN and commercial 20 wt% Pt/C were cycled from 0.6 V to 1.0 V with a sweep rate of 50 mV s^{-1}. After 5000 cycles, there was little change in the $E_{1/2}$ of Fe-ISAS/CN (*ca.* 4 mV), suggesting the superior stability of the ORR performance (Fig. 3e). By contrast, the 20 wt% commercial Pt/C had a poor stability with a 25 mV decay after 5000 cycles (Fig. S14†). To test the methanol tolerance ability, we compared the LSV curves of Fe-ISAS/CN in O_2-saturated 0.1 M KOH with and without 1.0 M CH_3OH. As shown in Fig. 3f, there is no obvious change in the $E_{1/2}$ after injection of CH_3OH, demonstrating the excellent methanol tolerance ability. In contrast, for 20 wt% commercial Pt/C the cathodic peak for oxygen reduction disappeared while an obvious peak for methanol oxidation appeared after injection of a 1.0 M CH_3OH solution (Fig. S15†), indicating its poor methanol tolerance.

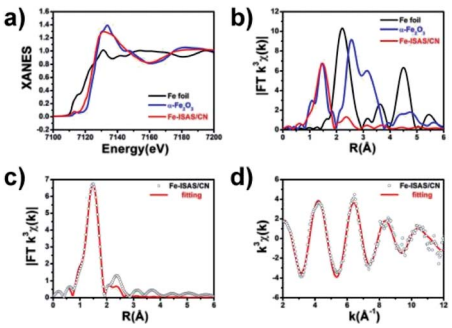

Fig. 2 (a) XANES spectra of Fe-ISAS/CN, Fe foil and α-Fe_2O_3 at the Fe K-edge. (b) Fourier transform (FT) spectra at the Fe K edge of Fe-ISAS/CN, Fe foil and α-Fe_2O_3. (c and d) The fitting results of the EXAFS spectra of Fe-ISAS/CN in *R* space and *k* space, respectively.

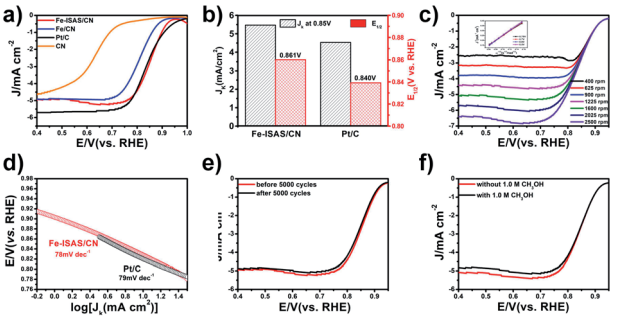

Fig. 3 (a) ORR polarization curves for different catalysts. (b) J_k at 0.85 V and $E_{1/2}$ of Fe-ISAS/CN and commercial 20 wt% Pt/C. (c) ORR polarization curves at different rotating rates of Fe-ISAS/CN. (d) The comparison of the Tafel slopes of Fe-ISAS/CN and commercial 20 wt% Pt/C. (e) ORR polarization curves of Fe-ISAS/CN before and after 5000 cycles. (f) ORR polarization curves of Fe-ISAS/CN without and with 1.0 M CH_3OH in O_2-saturated 0.1 M KOH.

This journal is © The Royal Society of Chemistry 2020

Open Access Article. Published on 30 November 2019. Downloaded on 8/23/2024 6:18:58 AM.
This article is licensed under a Creative Commons Attribution-NonCommercial 3.0 Unported Licence.

Except for electro-catalysis, the Fe-ISAS/CN also exhibited outstanding catalytic performance in organic reactions. Selective oxidation of ethylbenzene to acetophenone and dehydrogenation of 1,2,3,4-tetrahydroquinoline served as two model reactions to evaluate the reactivity of Fe-ISAS/CN. In the selective oxidation of ethylbenzene to acetophenone, the Fe-ISAS/CN showed high conversion (99%) and high selectivity (99%). The comparison of catalytic performance for the selective oxidation of ethylbenzene between Fe-ISAS/CN and other reported catalysts is listed in Table S4.† By contrast, the ultrathin Fe nanoparticles supported on the CN substrate (Fe-NPs/CN), (the corresponding HAADF-STEM images are shown in Fig. S16†), CN and the blank experiment without catalysts exhibited inferior conversion and poor selectivity (Fig. 4a), demonstrating that the outstanding catalytic performance for selective oxidation of ethylbenzene to acetophenone was attributed to the existence of Fe ISASs rather than Fe nanoparticles or COF-derived CN. After 5 cycles, the Fe-ISAS/CN still exhibited high reactivity with 87% conversion of ethylbenzene and excellent selectivity (99%) toward acetophenone (Fig. 4b), indicating that Fe-ISAS/CN had good recyclability. After the cycling test, the Fe atoms still existed in the ISAS form, which was confirmed by the results of HAADF-STEM, XANES and EXAFS measurements (Fig. S17 and S18†).

For the dehydrogenation of 1,2,3,4-tetrahydroquinoline, the Fe-ISAS/CN showed excellent activity and selectivity, with 100% conversion and 100% selectivity toward quinolone (Fig. 4c), and was superior to Fe-NPs/CN, CN and the blank experiment without catalysts. The comparison of catalytic performance for dehydrogenation of 1,2,3,4-tetrahydroquinoline between Fe-ISAS/CN and other reported catalysts is shown in Table S5.† After 5 cycles, the conversion was 82% and the selectivity was 100%, indicating the good recyclability of Fe-ISAS/CN (Fig. 4d). After cycling, the atomic dispersion of Fe atoms was confirmed by a combination of HAADF-STEM observation and XANES and EXAFS analysis (Fig. S19 and S20†).

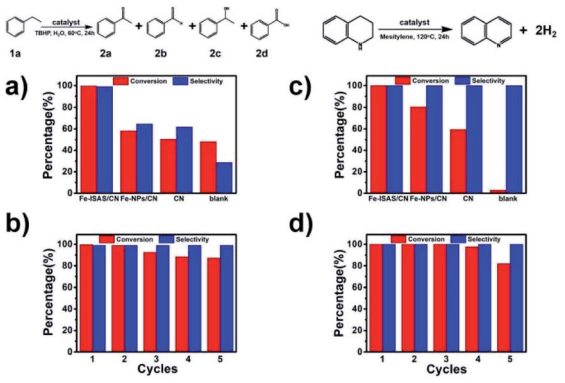

Fig. 4 (a) The comparison of the catalytic performance of Fe-ISAS/CN, Fe-NPs/CN, CN and the blank experiment without catalysts in the selective oxidation of ethylbenzene to acetophenone. (b) The recycling performance of the Fe-ISAS/CN catalyst in the selective oxidation of ethylbenzene to acetophenone. (c) The comparison of the catalytic performance of Fe-ISAS/CN, Fe-NPs/CN, CN and the blank experiment without catalysts in the dehydrogenation of 1,2,3,4-tetrahydroquinoline. (d) The recycling performance of the Fe-ISAS/CN catalyst in the dehydrogenation of 1,2,3,4-tetrahydroquinoline.

Conclusions

In summary, the Fe-ISAS/CN catalyst was obtained by a COF-absorption–pyrolysis strategy, which was also applicable to the synthesis of Co-ISAS/CN and Ni-ISAS/CN, demonstrating that it is a general method to prepare non-noble metal ISAS catalysts. The Fe-ISAS/CN catalyst can serve as an efficient multi-functional catalyst not only in electro-catalysis but also in organic catalysis. The Fe-ISAS/CN exhibited better ORR activity than commercial 20 wt% Pt/C, with good stability and methanol tolerance. In the selective oxidation of ethylbenzene and dehydrogenation of 1,2,3,4-tetrahydroquinoline, the Fe-ISAS/CN also exhibited outstanding reactivity with high conversion, high selectivity, and good recyclability and stability. This work will provide new insight into the synthesis of metal ISAS catalysts anchored on a COF-based substrate as multi-functional catalysts.

Conflicts of interest

There are no conflicts to declare.

Acknowledgements

This work was supported by the National Key R&D Program of China (2018YFA0702003), the National Natural Science Foundation of China (21890383, 21971137) and Beijing Municipal Science & Technology Commission No. Z191100007219003. We thank the BL14W1 station of the Shanghai Synchrotron Radiation Facility (SSRF) and 1W1B station at the Beijing Synchrotron Radiation Facility (BSRF) for the XAFS measurements.

Notes and references

1 B. Qiao, A. Wang, X. Yang, L. F. Allard, Z. Jiang, Y. Cui, J. Liu, J. Li and T. Zhang, *Nat. Chem.*, 2011, **3**, 634–641.
2 P. Liu, Y. Zhao, R. Qin, S. Mo, G. Chen, L. Gu, D. M. Chevrier, P. Zhang, Q. Guo, D. Zang, B. Wu, G. Fu and N. Zheng, *Science*, 2016, **352**, 797–801.
3 X. Yang, A. Wang, B. Qiao, J. Li, J. Liu and T. Zhang, *Acc. Chem. Res.*, 2013, **46**, 1740–1748.
4 L. Liu and A. Corma, *Chem. Rev.*, 2018, **118**, 4981–5079.
5 Y. Chen, S. Ji, C. Chen, Q. Peng, D. Wang and Y. Li, *Joule*, 2018, **2**, 1242–1264.
6 A. Han, B. Wang, A. Kumar, Y. Qin, J. Jin, X. Wang, C. Yang, B. Dong, Y. Jia, J. Liu and X. Sun, *Small Methods*, 2019, 1800471.
7 M. Zhang, Y.-G. Wang, W. Chen, J. Dong, L. Zheng, J. Luo, J. Wan, S. Tian, W.-C. Cheong, D. Wang and Y. Li, *J. Am. Chem. Soc.*, 2017, **139**, 10976–10979.
8 W. Liu, L. Zhang, X. Liu, X. Liu, X. Yang, S. Miao, W. Wang, A. Wang and T. Zhang, *J. Am. Chem. Soc.*, 2017, **139**, 10790–10798.

Open Access Article. Published on 30 November 2019. Downloaded on 8/23/2024 6:18:58 AM.
This article is licensed under a Creative Commons Attribution-NonCommercial 3.0 Unported Licence.

9 Y. Zhu, W. Sun, J. Luo, W. Chen, T. Cao, L. Zheng, J. Dong, J. Zhang, M. Zhang, Y. Han, C. Chen, Q. Peng, D. Wang and Y. Li, *Nat. Commun.*, 2018, **9**, 3861–3869.

10 Y. Han, Z. Wang, R. Xu, W. Zhang, W. Chen, L. Zheng, J. Zhang, J. Luo, K. Wu, Y. Zhu, C. Chen, Q. Peng, Q. Liu, P. Hu, D. Wang and Y. Li, *Angew. Chem., Int. Ed.*, 2018, **57**, 11262–11266.

11 W. Liu, L. Zhang, W. Yan, X. Liu, X. Yang, S. Miao, W. Wang, A. Wang and T. Zhang, *Chem. Sci.*, 2016, **7**, 5758–5764.

12 H. Su, P. Gao, M.-Y. Wang, G.-Y. Zhai, J.-J. Zhang, T.-J. Zhao, J. Su, M. Antonietti, X.-H. Li and J.-S. Chen, *Angew. Chem., Int. Ed.*, 2018, **57**, 15194–15198.

13 X. Dai, Z. Chen, T. Yao, L. Zheng, Y. Lin, W. Liu, H. Ju, J. Zhu, X. Hong, S. Wei, Y. Wu and Y. Li, *Chem. Commun.*, 2017, **53**, 11568–11571.

14 N. Cheng, L. Ren, X. Xu, Y. Du and S. X. Dou, *Adv. Energy Mater.*, 2018, 1801257.

15 X. Wang, W. Chen, L. Zhang, T. Yao, W. Liu, Y. Lin, H. Ju, J. Dong, L. Zheng, W. Yan, X. Zheng, Z. Li, X. Wang, J. Yang, D. He, Y. Wang, Z. Deng, Y. Wu and Y. Li, *J. Am. Chem. Soc.*, 2017, **139**, 9419–9422.

16 Q. Yang, C.-C. Yang, C.-H. Lin and H.-L. Jiang, *Angew. Chem., Int. Ed.*, 2019, **58**, 3511–3515.

17 Y. Qu, Z. Li, W. Chen, Y. Lin, T. Yuan, Z. Yang, C. Zhao, J. Wang, C. Zhao, X. Wang, F. Zhou, Z. Zhuang, Y. Wu and Y. Li, *Nat. Catal.*, 2018, **1**, 781–786.

18 S. Wei, A. Li, J.-C. Liu, Z. Li, W. Chen, Y. Gong, Q. Zhang, W.-C. Cheong, Y. Wang, L. Zheng, H. Xiao, C. Chen, D. Wang, Q. Peng, L. Gu, X. Han, J. Li and Y. Li, *Nat. Nanotechnol.*, 2018, **13**, 856–861.

19 P. Yin, T. Yao, Y. Wu, L. Zheng, Y. Lin, W. Liu, H. Ju, J. Zhu, X. Hong, Z. Deng, G. Zhou, S. Wei and Y. Li, *Angew. Chem., Int. Ed.*, 2016, **55**, 10800–10805.

20 L. Chen, L. Zhang, Z. Chen, H. Liu, R. Luque and Y. Li, *Chem. Sci.*, 2016, **7**, 6015–6020.

21 D. Wu, Q. Xu, J. Qian, X. Li and Y. Sun, *Chem.–Eur. J.*, 2019, **25**, 3105–3111.

22 Q. Li, W. Chen, H. Xiao, Y. Gong, Z. Li, L. Zheng, X. Zheng, W. Yan, W.-C. Cheong, R. Shen, N. Fu, L. Gu, Z. Zhuang, C. Chen, D. Wang, Q. Peng, J. Li and Y. Li, *Adv. Mater.*, 2018, 1800588.

23 A. Han, W. Chen, S. Zhang, M. Zhang, Y. Han, J. Zhang, S. Ji, L. Zheng, Y. Wang, L. Gu, C. Chen, Q. Peng, D. Wang and Y. Li, *Adv. Mater.*, 2018, 1706508.

24 C. Zhao, Y. Wang, Z. Li, W. Chen, Q. Xu, D. He, D. Xi, Q. Zhang, T. Yuan, Y. Qu, J. Yang, F. Zhou, Z. Yang, X. Wang, J. Wang, J. Luo, Y. Li, H. Duan, Y. Wu and Y. Li, *Joule*, 2019, **3**, 1–11.

25 Z.-Y. Wu, S.-L. Xu, Q.-Q. Yan, Z.-Q. Chen, Y.-W. Ding, C. Li, H.-W. Liang and S.-H. Yu, *Sci. Adv.*, 2018, **4**, eaat0788.

26 S. Han, H. Furukawa, O. M. Yaghi and W. A. Goddard, *J. Am. Chem. Soc.*, 2008, **130**, 11580–11581.

27 H. Furukawa and O. M. Yaghi, *J. Am. Chem. Soc.*, 2009, **131**, 8875–8883.

28 C. J. Doonan, D. J. Tranchemontagne, T. G. Glover, J. R. Hunt and O. M. Yaghi, *Nat. Chem.*, 2010, **2**, 235–238.

29 C. Montoro, D. Rodríguez-San-Miguel, E. Polo, R. Escudero-Cid, M. L. Ruiz-González, J. A. R. Navarro, P. Ocón and F. Zamora, *J. Am. Chem. Soc.*, 2017, **139**, 10079–10086.

30 J. Romero, D. Rodriguez-San-Miguel, A. Ribera, R. Mas-Ballestè, T. F. Otero, I. Manet, F. Licio, G. Abellàn, F. Zamora and E. Coronado, *J. Mater. Chem. A*, 2017, **5**, 4343–4351.

31 L. Stegbauer, K. Schwinghammer and B. V. Lotsch, *Chem. Sci.*, 2014, **5**, 2789–2793.

32 P. Pachfule, S. Kandambeth, D. Díaz Díaz and R. Banerjee, *Chem. Commun.*, 2014, **50**, 3169–3172.

33 C. S. Diercks, S. Lin, N. Kornienko, E. A. Kapustin, E. M. Nichols, C. H. Zhu, Y. B. Zhao, C. J. Chang and O. M. Yaghi, *J. Am. Chem. Soc.*, 2018, **140**, 1116–1122.

34 A. P. Côté, A. I. Benin, N. W. Ockwig, M. O'Keeffe, A. J. Matzger and O. M. Yaghi, *Science*, 2005, **310**, 1166–1170.

35 Y. Chen, S. Ji, S. Zhao, W. Chen, J. Dong, W.-C. Cheong, R. Shen, X. Wen, L. Zheng, A. I. Rykov, S. Cai, H. Tang, Z. Zhuang, C. Chen, Q. Peng, D. Wang and Y. Li, *Nat. Commun.*, 2018, **9**, 5422–5433.

36 Y. Chen, S. Ji, Y. Wang, J. Dong, W. Chen, Z. Li, R. Shen, L. Zheng, Z. Zhuang, D. Wang and Y. Li, *Angew. Chem.*, 2017, **129**, 1–6.

37 Y. Han, Y. Wang, R. Xu, W. Chen, L. Zheng, A. Han, Y. Zhu, J. Zhang, H. Zhang, J. Luo, C. Chen, Q. Peng, D. Wang and Y. Li, *Energy Environ. Sci.*, 2018, **11**, 2348–2352.

This journal is © The Royal Society of Chemistry 2020